Defining recovery neurobiology of injured spinal cord by synthetic matrix-assisted hMSC implantation

Alexander E. Ropper[a,b,c,1], Devang K. Thakor[a,b,c,1], InBo Han[a,b,c,1,3], Dou Yu[a,b,c,1], Xiang Zeng[a,c], Jamie E. Anderson[a,c], Zaid Aljuboori[a,c], Soo-Woo Kim[a,4], Hongjun Wang[d], Richard L. Sidman[e,2], Ross D. Zafonte[b], and Yang D. Teng[a,b,c,2]

[a]Division of SCI Research, Veterans Affairs Boston Healthcare System, Boston, MA 02130; [b]Department of Physical Medicine & Rehabilitation, Harvard Medical School/Spaulding Rehabilitation Hospital, Charlestown, MA 02129; [c]Department of Neurosurgery, Harvard Medical School/Brigham and Women's Hospital, Boston, MA 02115; [d]Biomedical Engineering, Chemistry, and Biological Sciences, Stevens Institute of Technology, Hoboken, NJ 07030; and [e]Department of Neurology, Harvard Medical School/Beth Israel Deaconess Medical Center, Boston, MA 02215

Contributed by Richard L. Sidman, December 18, 2016 (sent for review October 3, 2016; reviewed by Marcin Majka and Paul R. Sanberg)

Mesenchymal stromal stem cells (MSCs) isolated from adult tissues offer tangible potential for regenerative medicine, given their feasibility for autologous transplantation. MSC research shows encouraging results in experimental stroke, amyotrophic lateral sclerosis, and neurotrauma models. However, further translational progress has been hampered by poor MSC graft survival, jeopardizing cellular and molecular bases for neural repair in vivo. We have devised an adult human bone marrow MSC (hMSC) delivery formula by investigating molecular events involving hMSCs incorporated in a uniquely designed poly(lactic-*co*-glycolic) acid scaffold, a clinically safe polymer, following inflammatory exposures in a dorsal root ganglion organotypic coculture system. Also, in rat T9–T10 hemisection spinal cord injury (SCI), we demonstrated that the tailored scaffolding maintained hMSC stemness, engraftment, and led to robust motosensory improvement, neuropathic pain and tissue damage mitigation, and myelin preservation. The scaffolded nontransdifferentiated hMSCs exerted multimodal effects of neurotrophism, angiogenesis, neurogenesis, antiautoimmunity, and antiinflammation. Hindlimb locomotion was restored by reestablished integrity of submidbrain circuits of serotonergic reticulospinal innervation at lumbar levels, the propriospinal projection network, neuromuscular junction, and central pattern generator, providing a platform for investigating molecular events underlying the repair impact of nondifferentiated hMSCs. Our approach enabled investigation of recovery neurobiology components for injured adult mammalian spinal cord that are different from those involved in normal neural function. The uncovered neural circuits and their molecular and cellular targets offer a biological underpinning for development of clinical rehabilitation therapies to treat disabilities and complications of SCI.

spinal cord injury | recovery neurobiology | mesenchymal stromal stem cell | PLGA | locomotion

Repair of neurotrauma, stroke, and neurodegenerative diseases remains an unmet medical demand because of their pathophysiological complexity and the limited spontaneous healing capacity of adult mammalian CNS. Human mesenchymal stromal stem cells (hMSCs) offer autologous transplantation feasibility (1–4) and have been studied both experimentally and clinically for traumatic brain injury (TBI) and spinal cord injury (SCI) (5–8). Although MSCs possess homeostatic and proneurogenic activities (7, 9), studies relying on neural transdifferentiation (i.e., putative differentiations of MSCs into neural cells without reentering the pluripotency phase) did not show long-term functional improvement in SCI models. The poor outcomes were attributed mainly to suboptimal survival of MSCs, leaving key therapeutic mechanisms undetermined (10). We previously established a 3D cell delivery technology by seeding neural stem cells (NSCs) in biodegradable polymer scaffolds that significantly improved donor efficacy and enabled investigation of NSC repair mechanisms in the damaged CNS (11, 12). In the present study, to test whether hMSCs might facilitate SCI recovery via multimodal actions of neural protection, plasticity, antiinflammation, and angiogenesis, rather than by transdifferentiation (7, 9, 11–14), we designed a unique microtexture poly(lactic-*co*-glycolic) acid (PLGA) scaffold that maintains the stemness of hMSCs and in an organotypic dorsal root ganglion (DRG) coculture system, determined that inflammatory agents would induce both antiinflammatory and proneurogenic actions of the scaffolded hMSCs. Moreover, the multifaceted effects of hMSCs in the scaffold-improved survival and stemness status were comprehensively studied in vivo to probe the cellular and circuitry components underlying the "recovery neurobiology" as a defined concept, of injured adult rat spinal cords.

Results

Characterization of Stem Cell Biology of hMSCs in Vitro. Following established protocols (3), we characterized the stemness status of hMSCs (MSCness) by the expression of representative markers and the capacity for phenotypic differentiation. The passage 6

Significance

We developed a platform technology to determine therapeutic mechanisms of human mesenchymal stromal stem cells (hMSCs) in a dorsal root ganglion coculture system and an intraspinal cord implantation model. The unique poly(lactic-*co*-glycolic) acid scaffolding augments hMSC stemness, engraftment, and function without neural transdifferentiation or mesenchymal lineage development, resulting in robust motosensory improvement, pain and tissue damage mitigation, and myelin preservation in adult rat spinal cord after injury. The scaffolded hMSC-derived neurotrophism, neurogenesis, angiogenesis, antiautoimmunity, and antiinflammation support the propriospinal network, neuromuscular junctions, and serotonergic reticulospinal reinnervation to activate the central pattern generator for restoring hindlimb locomotion. Our findings illuminate "recovery neurobiology"—i.e., the injured spinal cord may deploy polysynaptic neural circuits different from normal adulthood pathways for postinjury improvement.

Author contributions: Y.D.T. designed research; A.E.R. and D.K.T. participated in study design; R.L.S. and R.D.Z. participated in bench work and project development; A.E.R., D.K.T., I.H., D.Y., X.Z., J.E.A., Z.A., and Y.D.T. performed research; A.E.R., D.K.T., I.H., D.Y., X.Z., J.E.A., Z.A., S.-W.K., H.W., R.L.S., R.D.Z., and Y.D.T. analyzed data; S.-W.K. helped with statistical analysis; H.W. participated in early stage paper writing; A.E.R. and D.K.T. participated in paper writing; R.L.S. and R.D.Z. participated in paper writing and refinement; and Y.D.T. wrote and finalized the paper.

Reviewers: M.M., Jagiellonian University Medical College; P.R.S., University of South Florida.

The authors declare no conflict of interest.

[1]A.E.R., D.K.T., I.H., and D.Y. contributed equally to this work.

[2]To whom correspondence may be addressed. Email: yang_teng@hms.harvard.edu or richard_sidman@hms.harvard.edu.

[3]Present address: Department of Neurosurgery, CHA Bundang Medical Center, Seongnam-si 13496, Korea.

[4]Present address: Department of Immunology and Infectious Diseases, Harvard School of Dental Medicine, Boston, MA 02115.

This article contains supporting information online at www.pnas.org/lookup/suppl/doi:10.1073/pnas.1616340114/-/DCSupplemental.

www.pnas.org/cgi/doi/10.1073/pnas.1616340114

(P6) hMSCs all expressed CD90 and CD105 markers (Fig. S1 *A* and *B*) and were capable of adipogenic, osteogenic, and chondrogenic differentiations as determined by Oil Red O (Fig. S1 *C–F*), Alizarin Red S (Fig. S1 *G–I*), and Alcian Blue staining (Fig. S1 *K* and *L*), respectively. hMSCs of P9–P12 also demonstrated definitive adipogenic differentiation, although in reduced levels compared with that of P6 cells (Fig. S1*C*). Additionally, real-time PCR was used to evaluate the adipogenic and osteogenic potencies of hMSCs by quantifying mRNA levels of adiponectin (Fig. S1*D*) and alkaline phosphatase (Fig. S1*J*), respectively. P8 cells showed significantly higher folds of mRNA expressions than P11 hMSCs undergoing differentiation. To test our hypothesis that homeostatic restoration of the host environment is a characteristic therapeutic impact of progenitor cells (9, 11), P6–P12 and P5–P7 hMSCs were used for the present in vitro and in vivo experiments, respectively (3, 13, 15).

Antiautoimmunity Actions of Scaffolded hMSCs Determined in Vitro. In addition to expressing immunosuppressive factors (e.g., IL-10, TGF-β, prostaglandin E2), hMSCs, after inflammatory insults, increase the expression of indoleamine 2,3-dioxygenase (IDO) that catabolizes tryptophan into kynurenine, picolinic acid, and quinolinic acid, resulting in tryptophan depletion. The combinatorial outcomes drastically eliminate the activated T-cells through apoptosis (15, 16). Although autoimmunity-triggered myelin loss has been reported to contribute to post-SCI disability (17), whether the IDO-mediated immunosuppressive effect is beneficial for repair of injured spinal cord remained to be investigated (18). We herein examined if IDO expression in hMSCs could be induced following direct exposure to the inflammatory mediator LPS, a trigger of autoimmune pathology, or to IFN-γ, a crucial factor for innate and adaptive immunity (19, 20). We found that a period of 2- or 24-h exposure to LPS and INF-γ, respectively, resulted in high levels of IDO expression in the hMSCs (Fig. 1*A*; $P < 0.01$), compared with negative IDO immunoreactivity (IR) in the control cells. Similarly, the same regimens of LPS and INF-γ stimulation significantly augmented IDO production in the PLGA-scaffolded hMSCs (Fig. 1*B*; $P < 0.01$), validating the study design to examine the construct's immunomodulatory effect in injured spinal cord (21).

Neurotherapeutic Mechanisms of PLGA-Scaffolded hMSCs Assessed in an Organotypic Coculture System. To counteract the paucity of well-characterized biomimetic models that permit effective in vitro screening of the complex mechanisms underlying adult stem cell-mediated neural benefits, we established an organotypic DRG and stem cell coculture assay by plating hMSCs around adult rat DRG explants (*Materials and Methods*). Such coculture settings induced neurite outgrowth from axonomized DRG neurons. The regenerating DRG neurites responded to hMSCs by changing their path to track and home toward hMSCs in closest proximity (Fig. 1 *C–E*), in contrast to neurite behavior in a DRG-alone preparation, where the less-regrown neurites manifested a nontargeted projection pattern (Fig. 1*F*). We quantitatively compared the projection trajectory of neurite extension between the emergent segment and the terminal tip of the DRG after 48 h of coculture. The angle between the neurite directions at the two locations was taken as a measure of hMSCs' neurotropic potency. Whereas the control DRG (cultured alone) showed an average neurite trajectory angle of 48.15° without targeting preference, DRG cocultured with hMSCs showed a significantly increased average neurite path angle of 59.25° ($P = 0.026$ relative to controls, Student's *t* test), further diverging from the original trajectory to home toward hMSCs (Fig. 1*G*).

We next investigated whether this DRG axonal extension/homing was influenced by hMSC secretion of neurotropic and neurotrophic molecules. A unique type of PLGA scaffold with fine-tuned softness, smoothness, and pore size ranges (see details in *Materials and Methods*) was synthesized to maximize their protection of hMSC viability and stemness that are crucial for the functional multipotency of stem cells (9–13). Survival of seeded hMSCs with characteristic spreading morphology was supported by the tailored scaffold (Fig. S2*A*), and these hMSCs expressed BDNF and CD90 (Fig. S2 *B* and *C*), indicating neurotrophic/tropic factor production and stemness maintenance (3).

In the organotypic DRG coculture system, hMSCs scaffolded in PLGA or PLGA coated with hMSC medium alone as controls were placed alternately 2 mm away from either the proximal or distal axotomy side of each explanted DRG. After 48-h culture, the length of regenerated neurites in cocultures was measured (e.g., scaffolded hMSC side: Fig. 1*H*; control side: Fig. 1*I*). We observed a significant increase in the mean length (22% increase, $P = 0.03$; Fig. 1*J*, *Upper*) and in the maximum absolute distance of growth (45% increase, $P = 0.03$; Fig. 1*J*, *Lower*) of neurites on the DRG side next to the scaffolded hMSCs in comparison with the opposite side exposed to the control scaffold alone. Moreover, the group average number of regrowing neurites was markedly increased on the side of DRG next to the scaffolded hMSCs, relative to the control side exposed to the control scaffold (288% increase; 98 ± 22 vs. 34 ± 6 neurites, $n = 6$; $P < 0.001$, paired Student's *t* test). We also found that cocultured hMSCs, either scaffolded or not, expressed ciliary neurotrophic factor (CNTF) and BDNF, potent neurogenic and neuroprotective molecules (Fig. 1 *K* and *L*). The secretion of CNTF showed a pattern of dependence on target exposure, and BDNF secretion by hMSCs was significantly increased by the presence of dissected/injured DRG explants relative to the scaffold-only controls ($P < 0.05$; one-way ANOVA; Fig. 1*I*). Overall, the data suggested that the active context/target-dependent biological responses (i.e., functional multipotency) of the scaffolded hMSCs may hold therapeutic potential for treating SCI (22).

Evaluation of Antiinflammatory Effects of Scaffolded hMSCs in Vitro. To simulate post-SCI inflammatory pathology (23) and evaluate the antiinflammatory potential of the scaffolded hMSCs, we challenged the organotypic DRG coculture system with LPS at 18 h after the assay initiation (20, 24). Following a dose escalation of LPS (20 pg/mL to 1,000 ng/mL), a graded increase of TNF-α expression was triggered; above the LPS dose of 1,000 ng/mL, TNF-α production in the DRG plateaued (Fig. S3*A*). DRG treated with 20 ng/mL LPS showed transient spikes of the proinflammatory cytokines TNF-α, IL-1β, and IL-6 expression, whereas coculture with PLGA-scaffolded hMSCs prevented these up-regulations (Fig. S3 *B–D*) by decreasing the group mean levels of mRNA expressions of TNF-α, IL-6, and IL-1β by 62%, 72%, and 65%, respectively (Fig. S3 *E–G*). The data demonstrated that we had established an in vitro cellular and molecular screening system for neural protection and repair events mediated by hMSCs (25).

Motosensory Recovery After SCI Resulting from Scaffolded hMSC Implantation in Vivo. To test our therapeutic device in lesioned spinal cord, the PLGA-scaffolded hMSC construct (Fig. 2*A*) was surgically implanted into the injury epicenter immediately following T9–T10 midline hemisection in female adult Sprague-Dawley rats (Fig. 2*B*) (11). We monitored behavioral recovery, focusing on locomotion and evolution of neuropathic pain as clinically relevant outcome measures. The mean Basso, Beattie, and Bresnahan (BBB) score [an established open-field locomotion scale ranging from 0 (paralysis) to 21 (normal)] for the hindlimb ipsilateral to the injury site in the scaffolded hMSC treatment group was significantly higher throughout the 4 wk after SCI relative to control groups that received hMSCs alone, lesion alone, or scaffold alone (Fig. 2*C*; $P < 0.05$, repeated-measures ANOVA; $n = 7$/group). All rats were immunosuppressed with Prograf; *Materials and Methods*). In addition, an inclined plane assay was performed to test forelimb strength (i.e., general physical condition) in the upward-facing orientation and

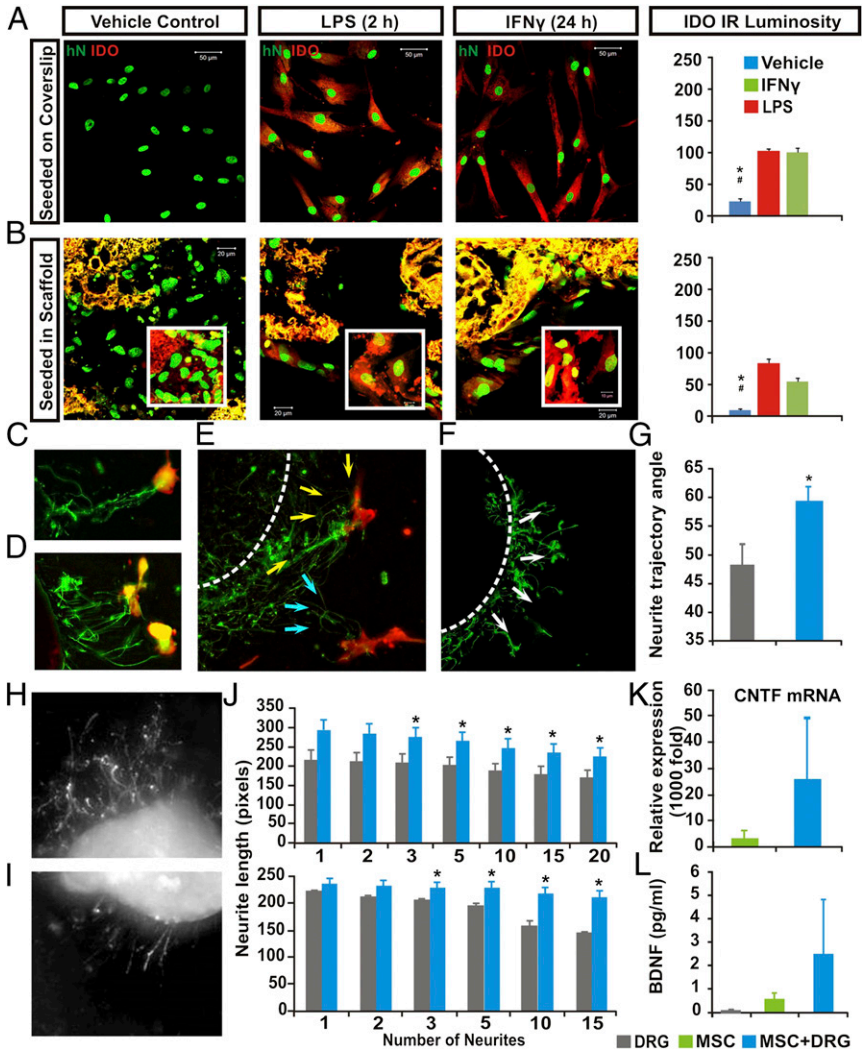

Fig. 1. Multimodal effects of hMSCs in vitro. Compared with saline control, LPS or IFN exposure significantly augmented IDO expression (red) in both (*A*) nonscaffolded hMSCs and (*B*) PLGA-scaffolded hMSCs, as shown by human nuclei (hN) immunostaining (green; $P < 0.05$: *, control vs. LPS; #, control vs. IFN-γ; $n = 5$; one-way ANOVA with Tukey's post hoc test). PLGA scaffolds showed yellow autofluorescence under dual channels. (*C–E*) DRG in organotypic coculture grew neurites (GAP43+, green) that track toward nearby hMSCs (CD90+, red; arrows), compared with (*F*) a more radial neurite pattern in DRG cultured with scaffold only (*G*). There were significantly more angular neurite paths in DRG and scaffolded hMSC cocultures (59.25 ± 2.9°) relative to the DRG and scaffold-alone group (48.15 ± 4.1°; $P = 0.026$, Student's *t* test). Images showed different lengths of neurite outgrowth at the (*H*) distal and (*I*) proximal sites of axotomized DRG cocultured with PLGA-scaffolded hMSCs or scaffold alone, respectively. (*J*, *Upper*) The scaffolded hMSC and DRG cocultures had significant increases in mean total lengths when 3–20 neurites per DRG were averaged (*$P = 0.032$, $n = 6$, Mann–Whitney) and also (*J*, *Lower*) significantly increased the maximum absolute length of DRG neurite outgrow when 3–15 neurites per DRG were assessed (*$P = 0.026$, $n = 6$, Mann–Whitney). (*K*) Relative CNTF mRNA expression in scaffolded hMSCs was significantly elevated, as was (*L*) secretion of human BDNF ($P < 0.05$, one-way ANOVA) in the scaffolded hMSC + DRG coculture system.

coordinated hindlimb motor function in the downward-facing orientation (11). The scaffolded hMSC-treated group achieved significantly higher (downward facing) inclined plane mean angle than all control groups (Fig. 2*D*), whereas no deficits in upward-facing performance were observed in any group.

For changes in spinal reflexes, by 4 wk post-SCI, 71% of the scaffolded hMSC-treated rats displayed a normal reflex response to a brief pressure stimulus to the affected hindlimb, whereas none (0%) of the lesion-only controls showed normal reflexes (Fig. 2*E*); importantly, 57% of the scaffolded hMSC-treated rats were able to perform a normal contact righting reflex, in contrast to 0% of the lesion-only controls (Fig. 2*F*). Thus, the scaffolded hMSC treatment was highly beneficial in recovering systemic (e.g., proprioception regarding contact righting) and local (e.g., brief pressure-induced spinal reflex) neural function in the SCI rats.

Sensory perturbations are common debilitating complications of clinical SCI. We evaluated the effects of scaffolded hMSC treatment on postinjury development of hypersensitivity, a type of sensory impairment associated with neuropathic pain conditions such as allodynia (26). The hindlimb response to a quick nociceptive pinch (i.e., pain withdrawal reflex) demonstrated a marked reduction in incidence rate of hyperreflexia in the scaffolded hMSC-treated rats, compared with the controls (Fig. 2*G*). For more detailed analyses, a barrage of sensory tests with standard 2- and 10-g Semmes-Weinstein filaments was performed weekly for each rat at approximately dermatomes T9–T10, as "at-level neuropathic pain," which is most frequently observed in clinical SCI (26). At 4 wk post-SCI, rats treated with scaffolded hMSCs demonstrated a significantly lower prevalence of hypersensitivity, relative to non–hMSC-treated controls (Fig. 2*H*), thus substantiating the therapeutic impact of scaffolded hMSC implantation for sensory disorders after SCI.

Histopathological Evaluation. Solvent blue and hematoxylin-stained spinal cord sections showed complete degradation of the PLGA scaffold in vivo ≥6 wk after SCI (Fig. 3*A*). Based on assessment of tissue sparing in representative spinal cords of each group (i.e., tissue from SCI rats with BBB scores closest to the group mean; $n = 4$ per group), the scaffolded hMSC treatment showed the most extensive neuroprotection. In addition to an overall difference among groups (one-way ANOVA, $P < 0.05$), the mean lesion volume was 3.99 mm^3 in the scaffolded hMSC group compared with 8.76 mm^3 in the lesion-only control group (~55% reduction in tissue loss; $P < 0.05$, Tukey's post hoc test; Fig. 3*B*). We also quantified the white matter volume (Fig. 3*C*, *Left*) and ventral horn motor neuron number (Fig. 3*D*, *Right*) of the spinal cord tissue sampled at 1-mm intervals rostral and/or caudal to the injury epicenter of the same set of spinal cords (27, 28). Relative to the controls, treatment with scaffolded hMSCs significantly spared white matter in tissue adjacent to the epicenter and enhanced the morphologic integrity of myelin determined by the solvent blue stain (27) (Fig. 3*C*, *Center* and *Right*, respectively);

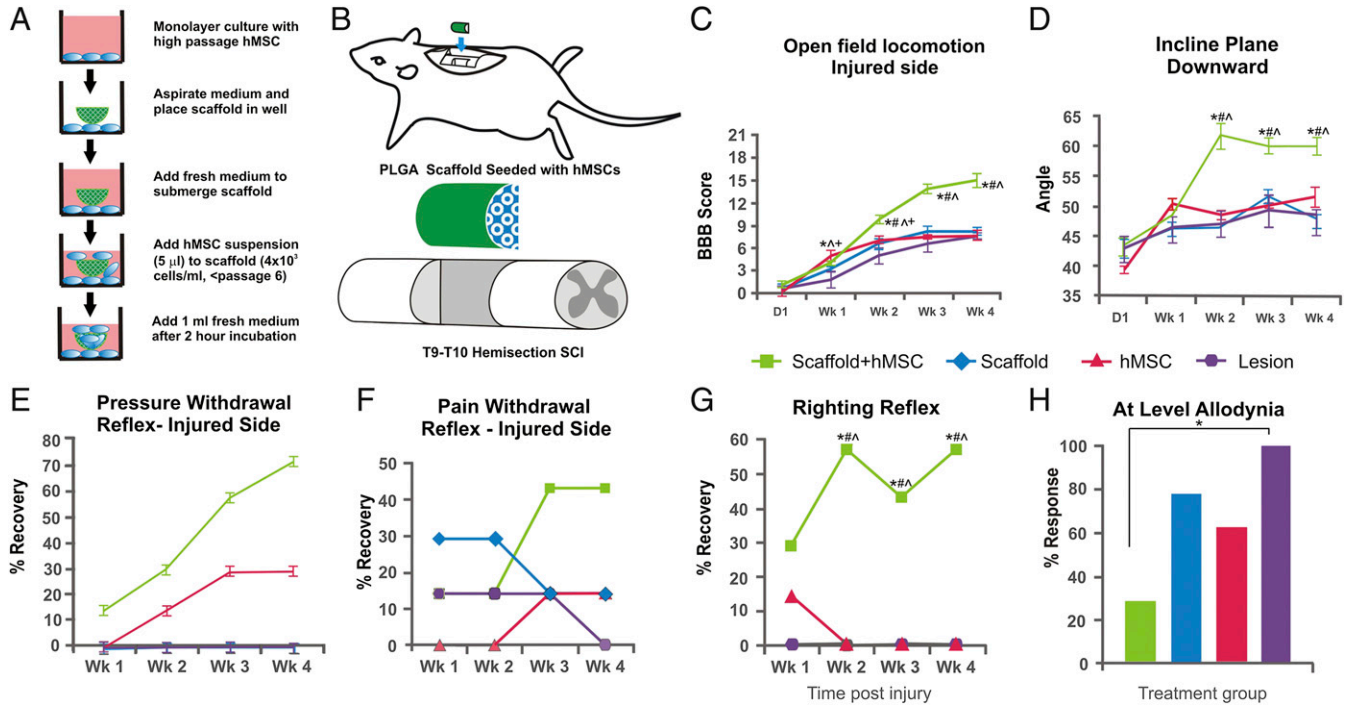

Fig. 2. Treatment designs and behavioral outcomes. Schematic presentations of (*A*) the in vitro hMSC seeding process for a PLGA scaffold and (*B*) design of the T9–T10 midline hemisection injury followed by implant insertion. Compared with three control groups, treatment with PLGA-scaffolded hMSCs significantly improved overall coordinated motor function as determined by (*C*) group mean BBB locomotion score of the hindlimb ipsilateral to injury and (*D*) inclined plane angle. Implantation of scaffolded hMSCs also significantly reduced occurrence of abnormal spinal reflexes in response to (*E*) pressure and (*G*) contact-triggered righting. Both (*F*) brief nociceptive pinch to the toe pads and (*H*) sensory tests at T9–T10 with standard 2- and 10-g Semmes-Weinstein filaments showed markedly higher hypersensitive responses in the controls relative to the scaffolded hMSC-treated rats (*, treated vs. lesion control, $P < 0.05$, Fisher's exact test). Data points ($n = 7$) represent average ± SEM or percent with normal (*E–G*) or abnormal (*H*) responses of each group, analyzed with repeated-measures ANOVA that showed an overall significant effect of treatment ($P < 0.05$). Symbols indicate that means are significantly different from those of the lesion-only (*), scaffold-only (#), and hMSCs-alone (^) control groups at the specified times after injury (Tukey's post hoc procedure or Student's *t* test).

it also significantly protected motor neurons in spinal cord loci caudal to the lesion epicenter (i.e., −1 to −4 mm; Fig. 3*D*, *Left*). We did not observe any ectopic growth/colonization or tumorigenesis of hMSCs in the CNS or in those internal organs collected (lungs, kidneys, liver, and spleen).

Fate and Multimodal Effects of Scaffolded hMSCs in Vivo. hMSC engraftment was evaluated immunocytochemically (ICC) for expression of human CD90 (hCD90) or human heat shock protein 27 (hHSP27) in adjacent sections. We found that in contrast to controls treated with nonscaffolded hMSCs that showed no long-term survival of donor cells, ICC-positive cells for hHSP27 or hCD90 were both detected in the scaffolded hMSC-treated spinal cords, with no statistical difference in the mean number between the two ICC markers (Fig. 4*A*), suggesting that the scored cells were of human origin with MSCness. The number of such hMSCs was highest at the lesion epicenter and sharply decreased within the surrounding 1–2 mm of host parenchyma in either direction, denoting the critical role of PLGA scaffolding for hMSC survival (11) and a strong tendency of hMSCs to remain close to the lesion epicenter. Surviving hMSCs at the injury site even at ∼6 wk postinjury was, on average, ≤2–5% of the cell number implanted. These hMSCs distributed slightly more in the rostral compared with the caudal side of the epicenter, a pattern similar to that reported previously for motor neuron sparing at T8 contusion epicenter (28).

The functional multipotent status of hMSCs was ICC assessed by their expression of therapeutic mediators (Fig. 1 and Figs. S2 and S3) (9, 11, 15). Relative to the controls, BDNF expression was increased more than threefold ($P < 0.05$, one-way ANOVA with post hoc Student's *t* test) in spinal cords of rats bearing scaffolded hMSCs (Fig. 4*B*, *Right*), elucidated in costaining for hHSP27 and DAPI (Fig. 4*B*). Expression of IL-10 (Fig. 4*C*, *Right*) was significantly higher in scaffolded hMSC-treated than in control spinal cords ($P < 0.05$, one-way ANOVA), largely in the remaining hMSCs, in contrast to the very limited number of host cells that showed IL-10 IR in the hMSC-alone group (Fig. 4*C*). We next evaluated expression of collagens I, II, and IV by ICC to determine if phenotypic differentiation of hMSCs occurred in the spinal cords ≥6 wk after injury and implantation. The lack of detectable collagen presence, confirmed by confocal microscopy, suggested that hMSCs did not undergo terminal mesenchymal differentiation. Also, there were neither hMSCs-derived osteocytes determined by alkaline phosphatase (ALP) IR (Fig. 4*D*, *Bottom*) nor Oil Red O-stained adipocytes. Last, based on our established protocols (14), we found no hMSC-derived neurons, astrocytes, or oligodendrocytes [verified by MAB1273 (Chemicon) staining for human mitochondrial antigen].

To determine whether the neural repair outcomes were derived specifically from multimodal actions of hMSCs (25), we examined the immunoregulatory capability of hMSCs (Fig. 1 *A* and *B*) to impede T-cells in the subacutely injured spinal cord (i.e., 7–10 d post-SCI; $n = 3$ per group). Despite administration of Prograf, CD3+ T cells were still present in the subacutely lesioned control tissue (21); PLGA-scaffolded hMSCs survived well and markedly increased expression of IDO (Fig. 4*E*) in the subacute SCI tissue, resulting in discernibly diminished presence of CD3+ T-cells in the white and gray matter at the epicenter (15, 25) (Fig. 4 *F* and *G*) and significantly mitigated invasion of iNOS-carrying mononuclear leukocytes (21, 25, 29) (Fig. 4*H*), which likely helped to protect myelin integrity (Fig. 3*C*). Compared with the lesion control tissue,

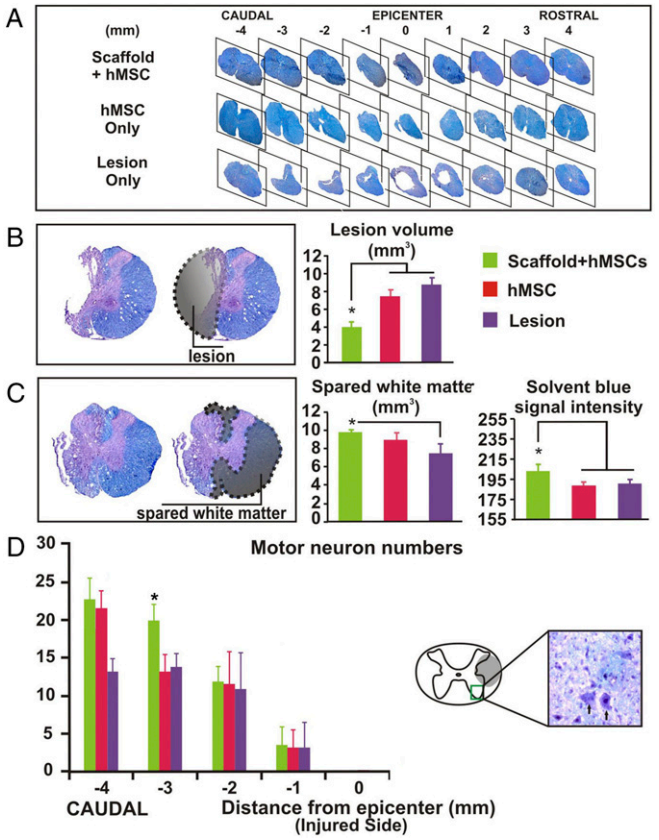

Fig. 3. Histopathological analysis. Solvent blue- and hematoxylin-stained serial transverse spinal cord sections showed (*A*) that spinal cords with implanted scaffolded hMSC had more spared tissue around the lesion site than hMSC-alone and lesion-only controls and complete degradation of the PLGA scaffolds at ≥6 wk after SCI. Quantitative assessment of representative spinal cords (n = 4 per group) showed that relative to the controls, (*B*) scaffolded hMSC significantly reduced mean lesion volume and (*C*) increased white matter sparing in the spinal cord sections ±2 mm from the lesion epicenter. (*D*) Scaffolded hMSC implantation also preserved ventral horn motor neurons (*Left*) in spinal cord tissue caudal to the epicenter. Asterisks indicate a significant difference from the control group ($P < 0.05$, one-way ANOVA or repeated-measures ANOVA with Tukey's post hoc test).

scaffolded hMSCs with high IDO expression levels significantly polarized macrophage toward an arginase 1-positive M2 phenotype (Fig. 4*H*, *Left* and *Center*) inducible by IDO-generated tryptophan catabolites and considered to be beneficial for neural repair (30), but reduced the number of activated microglia and macrophage (CD68+) in the subacute lesion epicenter (21) (Fig. 4*H*, *Right*). Moreover, we noted that most donor hMSCs appeared to have died off by chronic postinjury stages. Thus, the tailored scaffolding approach to implanting hMSCs into adult spinal cord niche may have the combinatorial effect of preventing lineage differentiation, neural transdifferentiation, and tumor formation of MSCs.

Impediment of Chronic Inflammation. The inflammatory cascade paradoxically contributes to both postinjury neural damage and repair (23, 31), so that subtly tuned antiinflammation capability has become a focus for treating CNS trauma (32–34). Based on the antiinflammatory and antiautoimmunity effects of scaffolded hMSCs in vitro (Fig. 1) and in vivo (Fig. 4), we assessed transverse sections at and adjacent to the lesion epicenter and found that GFAP, a marker of inflammation-triggered reactive astrogliosis (11), was lowest in spinal cords treated with scaffolded hMSCs (Fig. 5*A*). In addition, IR for nitrotyrosine (Fig. 5*B*), a "fingerprint" of protein nitration that indicates oxidative damage (29), was also significantly reduced in the treated spinal cords. Furthermore, ICC staining for CD68 (Fig. 5*C*), a marker of activated microglia and macrophages (35), was significantly decreased in chronic SCI tissue following treatment with scaffolded hMSCs, compared with control groups. Relative to the lesion-alone controls, the PLGA scaffold-only implant did not trigger discernibly worsened inflammatory responses in either subacutely or chronically injured spinal cords.

Neurobiological Mechanisms Underlying Post-SCI Recovery Following Implantation of Scaffolded hMSCs. We first investigated the impact of donor cells on endogenous NSCs (36) in the host spinal cord on the inference that established roles of mesoderm–ectoderm interaction during development (37, 38) might partly apply in adult injury repair, and the known neural repair effects of activated endogenous NSCs (9, 14). ICC analysis of doublecortin (DCX), a marker of migratory NSCs, revealed the presence of DCX+ NSCs that are normally absent in the intact adult mammalian spinal cord (39). We found (Fig. 5*D*) the number of DCX+ pixels in NSCs in the scaffolded hMSC-treated adult spinal cords 2 mm caudal to the lesion site to be significantly increased by ∼314%, compared with lesion-only or hMSC-only controls. Although activation by donor hMSCs of endogenous NSC proliferation, migration, and differentiation was previously described in the brain (36), the significant difference between the rats treated with scaffolded and nonscaffolded hMSCs suggests that a synthetic matrix tailored to enhance hMSC survival and stemness potently augmented the location-specific impact of hMSCs on adult spinal cord neurogenesis post-SCI, providing therapeutic benefits (9, 39). We also examined whether intraparenchymal angiogenesis, an important primary tissue repair mechanism that can be induced by MSCs (41), was promoted by the scaffolded hMSC implant around the epicenter; a nearly fourfold increase in group mean IR against laminin, a primary angiogenic marker (41), was detected by L9393, a pan anti-laminin antibody, in the treated spinal cords relative to the controls ($P < 0.05$; Fig. 5*E*). The laminin+ structures show morphologic features of blood vessels.

Because laminins, particularly those containing chains α2 and α5, are unique extracellular matrix protein components in the adult CNS neurogenic niche, and in addition to their effects on angiogenesis also promote neurite outgrowth (42), we investigated by ICC whether human laminin containing chains α2 and α5 was deposited by donor hMSCs around the epicenter. Indeed, (Fig. 5*F*, *i and ii*) these chains were secreted by scaffolded hMSCs around the implantation site in the subacutely injured spinal cord, and were present in the chronically injured tissue immediately caudal to the epicenter, forming (Fig. 5*F*, *iii*) an intertwined pattern of distribution with the sprouting serotonergic (5HT) neurites, indicating likely support for serotonergic reinnervation.

Our biotinylated dextran amine (BDA) anterograde tracing revealed no cross-epicenter regeneration of corticospinal tract (CST) axons in all spinal cord funiculi involved (e.g., Fig. 6 *A* and *C* showed the dorsal funiculus data) for all study groups. There was no evidence of rubrospinal tract (RST) regrowth beyond the lesion site, as determined (Fig. S4) by ICC of vGluT2, a primary marker of RST terminals (43). We thereby used a novel "peripheral–central" and "bottom-up" tracing strategy to elucidate the neural pathways responsible for the observed recovery of locomotion in the treated rats. We specifically investigated whether the rodent central pattern generator (CPG) for hindlimb locomotion might be partially activated by submidbrain inputs (40, 44); this was done by injecting different retrograde tracers [i.e., DiI, Fast Blue (FB), and Fluoro-Gold (FG)] into the cervical, thoracic, abdominal, and hindlimb muscles and performing 5HT ICC (Fig. 6 *A* and *B*; *Materials and Methods*) (40, 43, 44). We also immunochemically evaluated the distribution and quantity of synaptophysin, a pansynaptic vesicle protein and

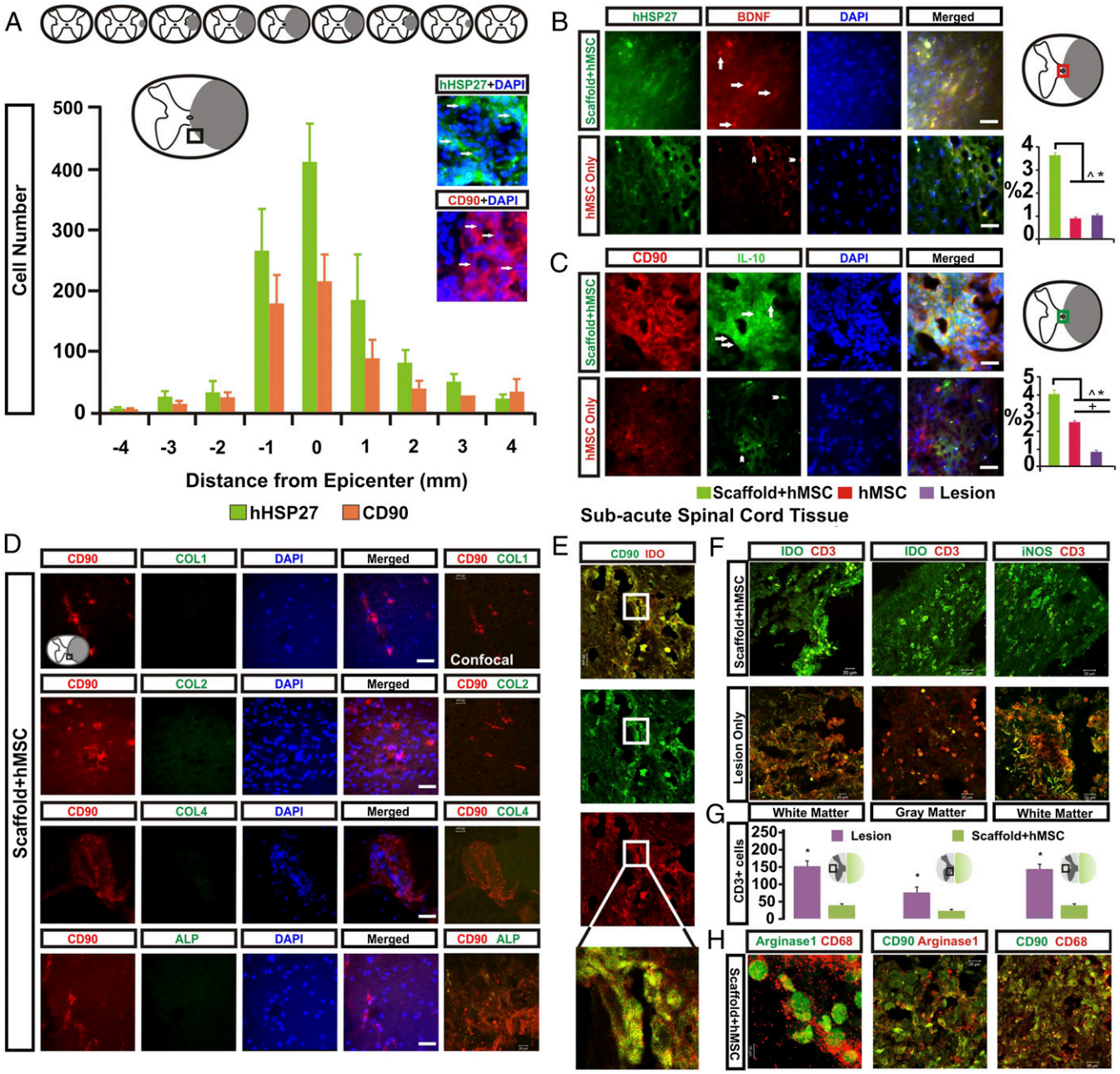

Fig. 4. Analysis of fate and multimodal effects of scaffolded hMSCs in vivo. (*A*) Immunostaining for CD90 and human heat shock protein 27 (hHSP27) showed long-term survival (≥6 wk postinjury) only of scaffolded hMSCs (arrowed cells in *Insets* for the framed area). The engrafted hMSCs were mostly CD90+ and primarily concentrated in the lesion epicenter, with sharply reduced presence in the adjacent parenchyma. (*B*) Costaining for hHSP27 demonstrated cytoplasmic BDNF in the engrafted hMSCs (*Left*); relative to the controls, mean expression level increased nearly fourfold in the scaffolded hMSC-treated group (*Right*: ^, comparing with hMSC alone or *, lesion only; $n = 5$ per group; $P < 0.05$). (*C*) Costaining for CD90 showed IL-10 expression in the engrafted hMSC cytoplasm (*Left*); expression level of IL-10 was significantly higher in the scaffolded hMSC-treated spinal cords (^, comparing with hMSC-only group and *, to lesion-only group; $^{+}$, hMSC only vs. lesion only; $n = 5$ per group; $P < 0.05$, one-way ANOVA with Tukey's post hoc test). (*D*) Confocal analysis of the scaffolded hMSC-treated spinal cord tissue detected no discernible IR to collagen I, II, and IV or ALP (bone tissue marker), despite persistent presence of CD90+ signals, suggesting that no mesenchymal phenotypic differentiation of hMSCs occurred in the injured spinal cords ≥6 wk after transplantation. (*E*) Confocal z-stack imaging confirmed that IDO was expressed mainly in the cytoplasm of donor hMSCs (CD90+, green) in the subacutely injured spinal cord (i.e., 7–10 d postinjury). (*F*) The number of infiltrated CD3+ (red) T-cells was significantly decreased (*G*) in the white matter areas 3 mm rostral (*Left*) and caudal (*Right*) to the epicenter, and in the gray matter 3 mm caudal to the epicenter (*G*, *Center*). (*H*) Scaffolded hMSCs (CD90+, green) discernibly increased the number of macrophages manifesting M2 phenotype polarization (arginase 1 IR: green), whereas the number of activated microglia and macrophage (CD68+) was greatly reduced near the epicenter of the subacutely injured spinal cord, compared with lesion-only or hMSC-alone controls ($n = 4$ per group).

vGluT1, the primary proprioceptive terminal glutamate transporter interacting with propriospinal interneurons (PSNs) in Rexed's Laminae (RL) IV–VIII and RL IX motor neurons (45). We found that compared with the lesion-only controls, the spinal cords treated with scaffolded hMSCs had a significantly stronger mean IR for synaptophysin around the ventral horn motor neurons at the cervical and thoracic segments with higher signal levels of DiI and FB (Fig. 6*D*), respectively, and of FG (Fig. 6*E*;

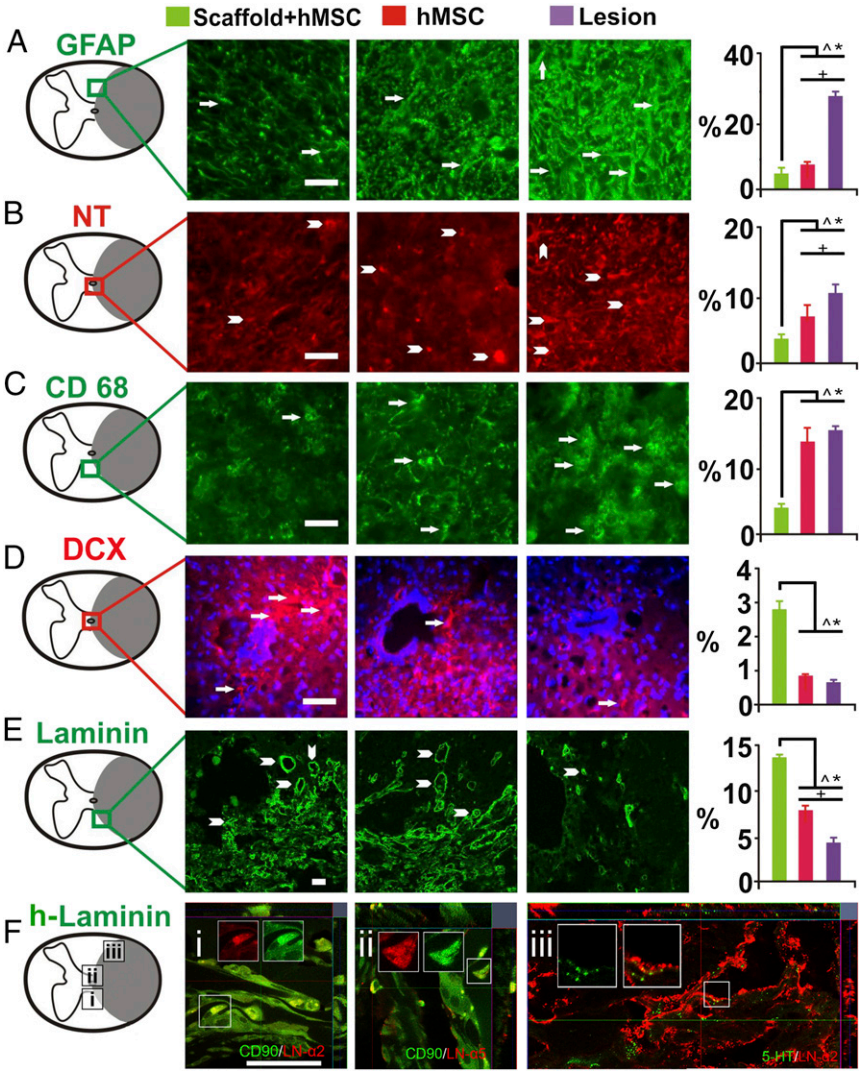

Fig. 5. Investigation of neural repair effects of scaffolded hMSC engraftment. Transverse spinal cord sections, 3 mm caudal to the injury epicenters, were immunostained for (*A*) GFAP for astrogliosis; (*B*) nitrotyrosine (NT) for oxidative damage; (*C*) CD68 for activated microglia (and vascular-derived macrophages); (*D*) DCX for endogenous NSCs; (*E*) laminin for angiogenesis; and (*F*) human laminin (h-laminin) to assess if donor hMSCs produced these glycoproteins to promote neurite outgrowth. The scaffolded hMSC treatment significantly reduced (*Right*) IR of GFAP, NT (protein nitration), and CD68. The treatment significantly augmented endogenous neurogenesis (arrows and arrowheads denote DCX+ NSCs in *D*) and increased angiogenesis in chronically lesioned spinal cord, indicated by the blood vessel-resembling morphology of pan-laminin IR (arrowheads in *E*). Moreover, h-laminin secretion from hMSCs (CD90+; green) near the epicenter in the subacutely injured spinal cord was detected (*F*, *i*: h-laminin α2 chain; *ii*: h-laminin α5 chain). Last, h-laminin deposition persisted chronically to ≥6 wk after injury in the same region (*F*, *iii*: h-laminin α2 chain) and showed intimate interactions with 5-HT+ axonal fibers, suggesting its promotion of serotonergic reinnervation (*F*, *iii*). (Scale bar: *A*–*D*, 50 μm: *E*, 20 μm; *F*, 25 μm.) $P < 0.05$, one-way ANOVA with Tukey's post hoc test: *, scaffolded hMSCs vs. lesion only; #, scaffolded hMSCs vs. hMSC alone, and $^{+}$, hMSC alone vs. lesion alone.

see statistics in Fig. 6*F*). The treated spinal cords also contained more 5HT+ fibers and vGluT1-positive buttons in the upper lumbar segments, suggesting improved plasticity of the propriospinal projection system that interacts actively with the 5HT+ reticulospinal fibers in the CPG region (Fig. 6*G*) (46–49). We also observed that at T10–T11, the engrafted and still undifferentiated hMSCs [i.e., stromal cell antigen 1 (STRO-1)+ cells] significantly augmented surrounding host cells' expression of connexin 43 (Cx43), the main gap junction-forming protein unit between neural cells, NSCs and inflammatory cells (32, 50), compared with controls (Fig. 6*H*). Notably, scaffolded hMSC-treated spinal cords, relative to controls, showed nearly normal T6–T8 dorsal horn innervation of primary proprioceptive fibers (Fig. 6*I*) and DRG neuronal integrity (Fig. 6*J*) as assessed by intramuscular retrograde tracers, and reduced degeneration of hindlimb neuromuscular junctions (NMJs: labeled by α-bungarotoxin; Fig. 6*K*). Clearly, the scaffolded hMSC-treated SCI rats showed an overall enhancement of the proprioceptive network and NMJ integrity, which might work together with improved descending serotonergic facilitation to reanimate CPG for locomotion recovery.

Discussion

We have developed an hMSC-delivering platform technology by seeding hMSCs in a uniquely designed PLGA matrix to improve donor cell survival in a nondifferentiated state and in a localized engraftment that fosters implant–host interaction in vivo. Developed concurrently is a neurotrauma-relevant DRG coculture system for in vitro screening of multiple neurotherapeutic effects of stem cells. Our synthetic matrix supports hMSC survival, stemness, and function, avoiding phenotypic differentiation, ectopic donor cell engraftment, and tumorigenesis in lesioned adult rat

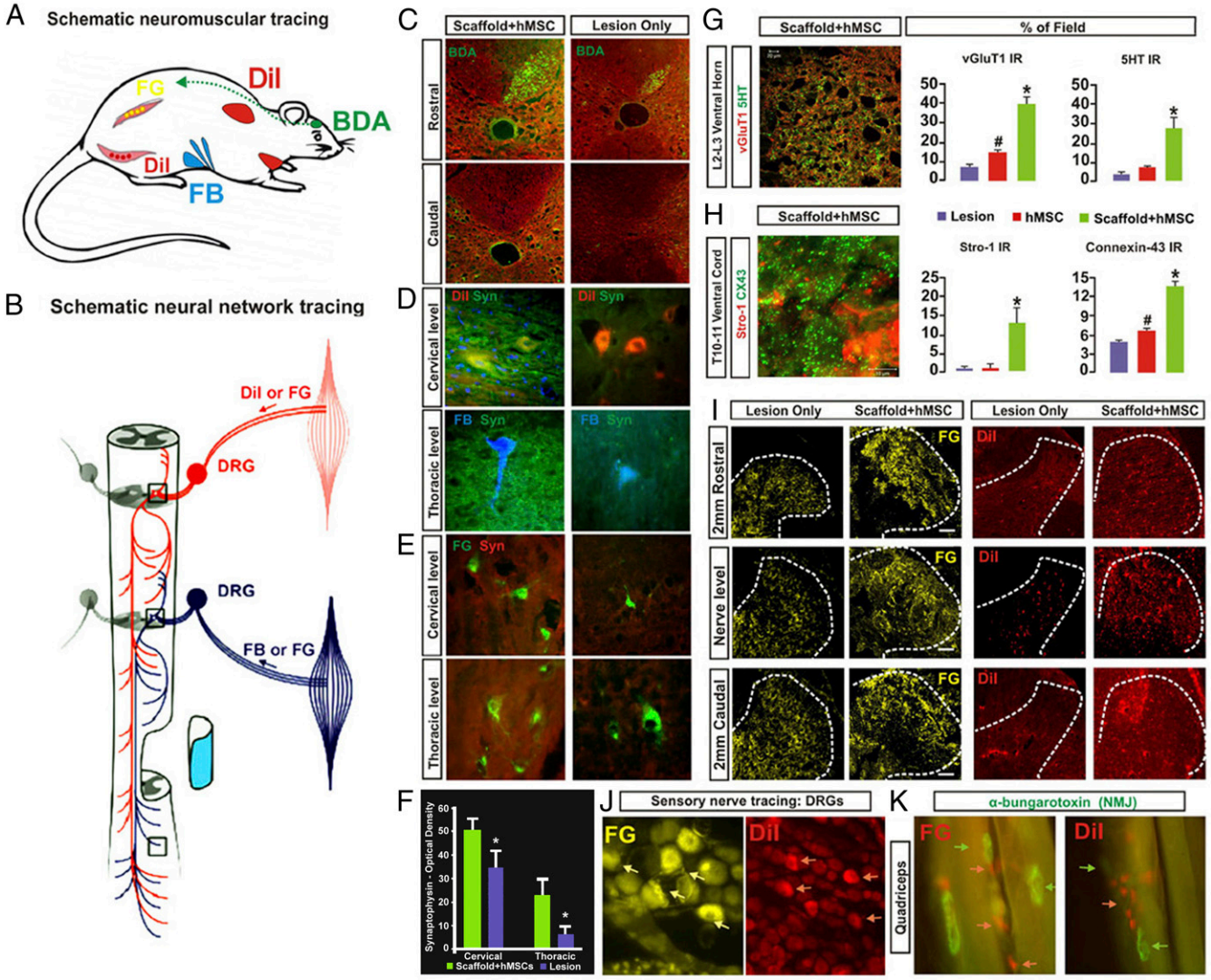

Fig. 6. Neurobiological benefits resulting from the scaffolded hMSC treatment. (*A*) Tracing regimens: BDA (green; injected into motosensory cortex contralateral to hemisection) for tracing the CST on the lesioned side, whereas DiI, Fast Blue (FB), and Fluoro-Gold (FG) were injected ipsilaterally into cervical region muscles and intercostal and abdominal muscles (*Materials and Methods*) to trace both primary proprioceptive axons that synapse with the PSN interneurons and with ventral horn motor neurons. DiI and FG were also injected into hindlimb muscles for retrograde tracing of lumbar motor neurons and primary afferent fibers. (*B*) Schematic of a simplified PSN network consisting of cross-segmental 1° and 2° neurites that project bilaterally and bidirectionally. (*C*) BDA IR was detected in the ipsilateral CST rostral to the injury epicenter, but not at any levels caudal to the lesion site in both scaffolded hMSC-treated and lesion-only spinal cords, suggesting no CST regeneration. (*D* and *E*) Images of DiI-, FB-, or FG-traced cervical and thoracic ventral horn motor neurons, respectively, and the synapses in the surrounding regions that were costained by antibody against synaptophysin (Syn, green), a synaptic vesicle marker. Scaffolded hMSCs-treated spinal cords showed much higher Syn IR density in both cervical and thoracic cord regions, compared with lesion-only (or hMSCs-only) controls (*F*; $P < 0.05$, paired Student's *t* test, $n = 5$ per group). (*G, Left*) Tissue slices selected from upper lumbar segment 5 mm caudal to the epicenter were immunostained for 5-HT (red) and vGluT1 (green). A representative z-stack confocal plane (20 × 0.1 μm optical sections) of the Rexed Lamina VIII area is shown (*Inset*) at 600× magnification, and presents typical details of the pericellular distribution of axon terminal vGluT1 and beaded varicosities of 5HT. (Scale bar: 5 μm.) (*G, Right*) Group average IR of vGluT1 (red) that marks primary proprioceptive terminals and 5HT (green) in lumbar Rexed Lamina VIII were significantly stronger in scaffolded hMSC-treated spinal cords compared with controls. (*H*) Coimmunostaining of STRO-1 (red), an hMSC marker and Cx43 (green), a gap junction protein, revealed significantly higher signal density of Cx43 in the host ventral cord region of sections immediately caudal to the scaffolded hMSC implant site, compared with the control groups (*, scaffolded hMSC vs. hMSC only and lesion only; #, hMSC only vs. lesion only; $P < 0.05$, $n = 5$ per group; one-way ANOVA with Tukey's post hoc test). Cx43 was expressed mainly by host cells (i.e., STRO-1–negative cells). (*I*) Retrograde tracing with FG or DiI via T6–T8 intercostal nerve showed FG+ or DiI+ primary afferent fibers and (*J*) DRG neurons. Scaffolded hMSC treatment drastically increased densities and area of both tracers, relative to the lesion controls, and DRG neuron integrity (*J*). (*K*) Motor nerve endings are in close contact with α-bungarotoxin+ nicotinic receptors in the muscles, showing near normal morphology of NMJs in the quadriceps of scaffolded hMSC-treated rats.

spinal cord. The scaffolded hMSCs implanted at a T9–T10 hemitransection site robustly restore locomotor function and prevent neuropathic pain by mitigating T-cell–mediated demyelination and augmenting M2 macrophage polarization, by providing BDNF, CNTF, and IL-10 cytokines, serotonergic neurite sprouting, and morphologic integrity of thoracolumbar synapses, and by promoting angiogenesis, endogenous neurogenesis, and gap junction formation. Notably, these biological effects were exerted by hMSCs in the progenitor state, without mesenchymal lineage differentiation or neural transdifferentiation. Thereby, hMSCs may provide their therapeutic impacts mainly through functional multipotency events, conducive to post-SCI

coordination of four components essential for hindlimb locomotor recovery: (*i*) serotonergic reticulospinal reinnervation caudal to the lesion; (*ii*) propriospinal projection network plasticity; (*iii*) NMJ integrity; and (*iv*) CPG reactivation (40, 43–45). In regard to CST axonal regrowth as the frequently pursued central regenerative goal in treating SCI, these outcomes collectively introduce a different theoretical and experimental platform to investigate stem cell-based therapy that sets forth an interactive set of recovery neurobiology mechanisms for lesioned adult mammalian spinal cord.

Although the T9–T10 lesion paradigm we used does not directly model spinal cord contusion, the most common SCI seen clinically, it offers the special opportunity to investigate precisely lesion scale, secondary injury, donor cell fate, neuroprotection, neurite outgrowth, and intraspinal cord pathway plasticity (11, 29, 46). Targeting each of the multiple pathophysiological mechanisms underlying SCI individually has to date yielded a high number of proposals, indicating their inadequacy and occasional mutual contradictions (48). We and others have proposed that the complexity and heterogeneity of SCI pathology necessitates development of multimodal integrated mechanistic and therapeutic regimens (11, 46, 48). We now consider the scaffolded hMSCs to represent an effective strategy based on the multiple therapeutic mechanisms observed in the present study, especially the cooperative effects of tissue sparing, serotonergic axonal sprouting, and propriospinal plasticity. Previously, implantation of a PLGA scaffold by itself that had different texture and composition tailored to enhance spinal cord healing significantly improved function in the same rat SCI model (11). By contrast, the matrix of the present formulation designed to maintain MSCness, when used by itself as an implant, was not sufficiently efficacious for post-SCI hindlimb recovery. Our data suggest that a correctly formulated synthetic matrix is crucial for realization of the intended biological effects without triggering side effects. The porous and flexible attributes of the current PLGA scaffold are essential for maintaining the basic stemness biology of hMSCs, avoiding unwanted mesenchymal differentiation. Compared with other types of polymers, PLGA offers reliable chemical engineering properties that can be adapted to optimize stem cell seeding and fate control (11). It has been reported lately that substrate stiffness could regulate the stemness level of progenitor cells (51). hMSCs under our delivery regimen exercised their homeostatic function while undifferentiated, and later died off, probably by apoptosis, because no necrosis-triggered inflammatory signs were spotted. This process may describe a desirable cell fate for nonneural progenitor cells serving for SCI treatment. The donor cells interacted with host cells to produce molecules that ameliorate local pathology. There was up-regulation of IDO, M2 polarization, endogenous neurogenesis, and gap junction formation, accompanied by down-regulation of proinflammatory cytokines, T-cells, and M1 macrophages (22, 23, 32, 39, 50), all in site-specific actions realized through tailored PLGA scaffolding of hMSCs and in a manner essentially unachievable for repairing open wounds by hMSC-conditioned medium or nonscaffolded cells. Hence, the notion of implanting stem cells pre- or postdifferentiated to a neural lineage may be working at cross-purposes to the developmental imperatives of the multipotent cells in certain cases, particularly for systemic repair of complex organs such as the spinal cord and brain (25, 32, 33). Our results suggest that scaffolded hMSCs may be adaptable for implantation directly into the contused spinal cord of patients in the subacute phase after injury when autoimmune and inflammatory insults peak (4, 33, 41, 48).

Traditional belief has attributed functional recovery observed after SCI in rodents primarily to the regrowth of CST and/or RST axons. Nevertheless, following thoracic lesion of descending motor pathways, neuroplasticity also occurs more caudally in the PSN network and lumbar CPG, a semiautonomous neural circuit for locomotion (45, 49). Studies examining "spinalized" cats or humans with incomplete SCI have demonstrated that motor cues, such as weight-suspended treadmill training or treadmill walk, can reanimate the CPG and its reengagement of arm swing, respectively (52, 53). Previously, a combinatorial application of direct electrical stimulation or administration of 5-HT receptor agonists enabled locomotion in spinalized rodents with dual spinal cord hemisections by igniting the PSN network for CPG activation through relaying CST signals (44). The present data, however, show that scaffolded delivery of hMSCs restored locomotor function in adult rats with T9–10 hemisection without promoting CST and RST regeneration across the injury epicenter or neural transdifferentiation of hMSCs. Our deductive analysis reveals that functional improvement of the affected hindlimb was likely supported by CPG activation via a submidbrain circuitry that is driven by treatment-enhanced reciprocal communication among the serotonergic reticulospinal pathway, PSN, and the neuromuscular system secured by NMJ preservation. We observed significantly increased IR of vGluT1 and synaptophysin expression and augmented presence of serotonergic fibers in RL IV–VIII around the epicenter and in RL IX of lumbar segments in the treated spinal cord relative to the controls. It was shown that after unilateral pyramidal tract section, proprioceptive fibers could sprout into the denervated motoneuron region as an evidence of maladaptive plasticity (54). By contrast, our results demonstrate that the enhanced PSN network, together with improved serotonergic reinnervation and preserved NMJs resulting from scaffolded hMSC implantation, exemplify beneficial plastic adaptations; this, combined with better preserved dorsal horn proprioceptive innervation, may serve as a pivotal mechanism to reactivate CPG and impede neuropathic pain following SCI. We are currently analyzing selective lesion data generated by targeted transgenic models in mice to verify the essential role of each specific neural component in recovering locomotion after SCI.

In conclusion, our findings corroborate the newly emerging observation that adult mammalian spinal cord contains inherent circuits that may be therapeutically recruited and modulated to restore function posttrauma (8, 49, 53, 55). These results collectively suggest it is plausible that direct axonal connections from motor cortex neurons to spinal cord are not essential for reestablishment of basic locomotion after mammalian SCI (55–57). Our results help define recovery neurobiology: the lesioned adult CNS may use neural circuits not identical to those deployed under normal physiological conditions for functional improvement. Therefore, SCI repair studies, in addition to pursuing regeneration of the CST and RST, should investigate recovery requirements that are specific for restoring targeted function. Tailored polymer scaffolding for hMSC delivery offers new opportunities for adult stem cell-based approaches to understanding and treating neurotrauma and perhaps other types of neural degeneration (58).

Materials and Methods

Experimental group size in the in vivo study was set at $n = 7$ per group based on power analysis of the outcome measure data of a previous study (28). All rats survived the entire study and were tested behaviorally at day 1 and then weekly after injury through ≥4 wk after injury. Remaining information is detailed in *SI Materials and Methods*.

All surgical procedures were performed in strict compliance with the Laboratory Animal Welfare Act and the *Guide for the Care of Use of Laboratory Animals* (59) after review and approval by the Institutional Animal Care and Use Committee of the VA Boston Healthcare System or Harvard Medical School.

ACKNOWLEDGMENTS. Support for this work was provided by United States Department of Veterans Affairs Rehabilitation Research and Development Grant 1-I01-RX000308-01A1, Center for the Advancement of Science in Space and National Aeronautics and Space Administration Grant GA-2015-222, CIMT-DoD Grant (to Y.D.T.), and a Cele H. and William B. Rubin Family Fund, Inc. Grant for the Gordon Program (to Y.D.T. and R.D.Z.).

1. Egusa H, et al. (2007) Downregulation of extracellular matrix-related gene clusters during osteogenic differentiation of human bone marrow- and adipose tissue-derived stromal cells. *Tissue Eng* 13(10):2589–2600.
2. Connick P, et al. (2012) Autologous mesenchymal stem cells for the treatment of secondary progressive multiple sclerosis: An open-label phase 2a proof-of-concept study. *Lancet Neurol* 11(2):150–156.
3. Lennon DP, Schluchter MD, Caplan AI (2012) The effect of extended first passage culture on the proliferation and differentiation of human marrow-derived mesenchymal stem cells. *Stem Cells Transl Med* 1(4):279–288.
4. Prockop DJ (2013) Concise review: Two negative feedback loops place mesenchymal stem/stromal cells at the center of early regulators of inflammation. *Stem Cells* 31(10): 2042–2046.
5. Parr AM, Tator CH, Keating A (2007) Bone marrow-derived mesenchymal stromal cells for the repair of central nervous system injury. *Bone Marrow Transplant* 40(7): 609–619.
6. Kumar AA, Kumar SR, Narayanan R, Arul K, Baskaran M (2009) Autologous bone marrow derived mononuclear cell therapy for spinal cord injury: A phase I/II clinical safety and primary efficacy data. *Exp Clin Transplant* 7(4):241–248.
7. Saito F, et al. (2012) Administration of cultured autologous bone marrow stromal cells into cerebrospinal fluid in spinal injury patients: A pilot study. *Restor Neurol Neurosci* 30(2):127–136.
8. Jarocha D, et al. (2014) Preliminary study of autologous bone marrow nucleated cells transplantation in children with spinal cord injury. *Stem Cells Transl Med* 3(3): 395–404.
9. Teng YD, et al. (2011) Functional multipotency of stem cells: A conceptual review of neurotrophic factor-based evidence and its role in translational research. *Curr Neuropharmacol* 9(4):574–585.
10. Alexanian AR, Kwok WM, Pravdic D, Maiman DJ, Fehlings MG (2010) Survival of neurally induced mesenchymal cells may determine degree of motor recovery in injured spinal cord rats. *Restor Neurol Neurosci* 28(6):761–767.
11. Teng YD, et al. (2002) Functional recovery following traumatic spinal cord injury mediated by a unique polymer scaffold seeded with neural stem cells. *Proc Natl Acad Sci USA* 99(5):3024–3029.
12. Park KI, Teng YD, Snyder EY (2002) The injured brain interacts reciprocally with neural stem cells supported by scaffolds to reconstitute lost tissue. *Nat Biotechnol* 20(11): 1111–1117.
13. Quertainmont R, et al. (2012) Mesenchymal stem cell graft improves recovery after spinal cord injury in adult rats through neurotrophic and pro-angiogenic actions. *PLoS One* 7(6):e39500.
14. Teng YD, et al. (2012) Multimodal actions of neural stem cells in a mouse model of ALS: a meta-analysis. *Sci Transl Med* 4(165):165ra164.
15. Ren G, et al. (2009) Species variation in the mechanisms of mesenchymal stem cell-mediated immunosuppression. *Stem Cells* 27(8):1954–1962.
16. Meisel R, et al. (2004) Human bone marrow stromal cells inhibit allogeneic T-cell responses by indoleamine 2,3-dioxygenase-mediated tryptophan degradation. *Blood* 103(12):4619–4621.
17. Lee KD, et al. (2009) FTY720 reduces inflammation and promotes functional recovery after spinal cord injury. *J Neurotrauma* 26(12):2335–2344.
18. Griffin MD, et al. (2013) Concise review: Adult mesenchymal stromal cell therapy for inflammatory diseases: How well are we joining the dots? *Stem Cells* 31(10): 2033–2041.
19. Schoenborn JR, Wilson CB (2007) Regulation of interferon-gamma during innate and adaptive immune responses. *Adv Immunol* 96:41–101.
20. Chastain EM, Miller SD (2012) Molecular mimicry as an inducing trigger for CNS autoimmune demyelinating disease. *Immunol Rev* 245(1):227–238.
21. Trivedi A, Olivas AD, Noble-Haeusslein LJ (2006) Inflammation and spinal cord injury: Infiltrating leukocytes as determinants of injury and repair processes. *Clin Neurosci Res* 6(5):283–292.
22. Cantinieaux D, et al. (2013) Conditioned medium from bone marrow-derived mesenchymal stem cells improves recovery after spinal cord injury in rats: An original strategy to avoid cell transplantation. *PLoS One* 8(8):e69515.
23. David S, Zarruk JG, Ghasemlou N (2012) Inflammatory pathways in spinal cord injury. *Int Rev Neurobiol* 106:127–152.
24. Kondo S, Kohsaka S, Okabe S (2011) Long-term changes of spine dynamics and microglia after transient peripheral immune response triggered by LPS in vivo. *Mol Brain* 4:27.
25. Ribeiro TB, et al. (2015) Neuroprotection and immunomodulation by xenografted human mesenchymal stem cells following spinal cord ventral root avulsion. *Sci Rep* 5: 16167.
26. Finnerup NB, et al. (2014) Phenotypes and predictors of pain following traumatic spinal cord injury: A prospective study. *J Pain* 15(1):40–48.
27. Rosenberg LJ, Teng YD, Wrathall JR (1999) 2,3-Dihydroxy-6-nitro-7-sulfamoyl-benzo (f)quinoxaline reduces glial loss and acute white matter pathology after experimental spinal cord contusion. *J Neurosci* 19(1):464–475.
28. Teng YD, Mocchetti I, Taveira-DaSilva AM, Gillis RA, Wrathall JR (1999) Basic fibroblast growth factor increases long-term survival of spinal motor neurons and improves respiratory function after experimental spinal cord injury. *J Neurosci* 19(16): 7037–7047.
29. Yu D, et al. (2009) Blockade of peroxynitrite-induced neural stem cell death in the acutely injured spinal cord by drug-releasing polymer. *Stem Cells* 27(5):1212–1222.
30. François M, Romieu-Mourez R, Li M, Galipeau J (2012) Human MSC suppression correlates with cytokine induction of indoleamine 2,3-dioxygenase and bystander M2 macrophage differentiation. *Mol Ther* 20(1):187–195.
31. Schwab JM, Zhang Y, Kopp MA, Brommer B, Popovich PG (2014) The paradox of chronic neuroinflammation, systemic immune suppression, autoimmunity after traumatic chronic spinal cord injury. *Exp Neurol* 258:121–129.
32. Cusimano M, et al. (2012) Transplanted neural stem/precursor cells instruct phagocytes and reduce secondary tissue damage in the injured spinal cord. *Brain* 135(Pt 2): 447–460.
33. DePaul MA, et al. (2015) Intravenous multipotent adult progenitor cell treatment decreases inflammation leading to functional recovery following spinal cord injury. *Sci Rep* 5:16795.
34. Scruggs BA, et al. (2013) Multipotent stromal cells alleviate inflammation, neuropathology, and symptoms associated with globoid cell leukodystrophy in the twitcher mouse. *Stem Cells* 31(8):1523–1534.
35. Yu D, et al. (2013) Alleviation of chronic pain following rat spinal cord compression injury with multimodal actions of huperzine A. *Proc Natl Acad Sci USA* 110(8): E746–E755.
36. Bao X, et al. (2011) Transplantation of human bone marrow-derived mesenchymal stem cells promotes behavioral recovery and endogenous neurogenesis after cerebral ischemia in rats. *Brain Res* 1367:103–113.
37. Henrique D, Abranches E, Verrier L, Storey KG (2015) Neuromesodermal progenitors and the making of the spinal cord. *Development* 142(17):2864–2875.
38. Haragopal H, et al. (2015) Stemness enhancement of human neural stem cells following bone marrow MSC coculture. *Cell Transplant* 24(4):645–659.
39. Sabelström H, et al. (2013) Resident neural stem cells restrict tissue damage and neuronal loss after spinal cord injury in mice. *Science* 342(6158):637–640.
40. Konya D, et al. (2008) Functional recovery in T13-L1 hemisected rats resulting from peripheral nerve rerouting: Role of central neuroplasticity. *Regen Med* 3(3):309–327.
41. Assi R, et al. (2016) Delivery of mesenchymal stem cells in biomimetic engineered scaffolds promotes healing of diabetic ulcers. *Regen Med* 11(3):245–260.
42. Kazanis I, et al. (2010) Quiescence and activation of stem and precursor cell populations in the subependymal zone of the mammalian brain are associated with distinct cellular and extracellular matrix signals. *J Neurosci* 30(29):9771–9781.
43. Du Beau A, et al. (2012) Neurotransmitter phenotypes of descending systems in the rat lumbar spinal cord. *Neuroscience* 227:67–79.
44. Courtine G, et al. (2009) Transformation of nonfunctional spinal circuits into functional states after the loss of brain input. *Nat Neurosci* 12(10):1333–1342.
45. Fukuhara K, et al. (2013) Specificity of monosynaptic sensory-motor connections imposed by repellent Sema3E-PlexinD1 signaling. *Cell Reports* 5(3):748–758.
46. Pritchard CD, et al. (2010) Establishing a model spinal cord injury in the African green monkey for the preclinical evaluation of biodegradable polymer scaffolds seeded with human neural stem cells. *J Neurosci Methods* 188(2):258–269.
47. Flynn JR, Graham BA, Galea MP, Callister RJ (2011) The role of propriospinal interneurons in recovery from spinal cord injury. *Neuropharmacology* 60(5):809–822.
48. Kwon BK, et al. (2011) A systematic review of directly applied biologic therapies for acute spinal cord injury. *J Neurotrauma* 28(8):1589–1610.
49. Angeli CA, Edgerton VR, Gerasimenko YP, Harkema SJ (2014) Altering spinal cord excitability enables voluntary movements after chronic complete paralysis in humans. *Brain* 137(Pt 5):1394–1409.
50. Jaderstad J, et al. (2010) Communication via gap junctions underlies early functional and beneficial interactions between grafted neural stem cells and the host. *Proc Natl Acad Sci U S A* 107(11):5184–5189.
51. Yang C, Tibbitt MW, Basta L, Anseth KS (2014) Mechanical memory and dosing influence stem cell fate. *Nat Mater* 13(6):645–652.
52. Lovely RG, Gregor RJ, Roy RR, Edgerton VR (1986) Effects of training on the recovery of full-weight-bearing stepping in the adult spinal cat. *Exp Neurol* 92(2):421–435.
53. Tester NJ, et al. (2011) Device use, locomotor training and the presence of arm swing during treadmill walking after spinal cord injury. *Spinal Cord* 49(3):451–456.
54. Tan AM, Chakrabarty S, Kimura H, Martin JH (2012) Selective corticospinal tract injury in the rat induces primary afferent fiber sprouting in the spinal cord and hyperreflexia. *J Neurosci* 32(37):12896–12908.
55. Kawai R, et al. (2015) Motor cortex is required for learning but not for executing a motor skill. *Neuron* 86(3):800–812.
56. Grillner S (2016) Role of motor cortex in movement challenged. *Curr Biol* 25: R490–R514.
57. Jarocha D, Milczarek O, Wedrychowicz A, Kwiatkowski S, Majka M (2015) Continuous improvement after multiple mesenchymal stem cell transplantations in a patient with complete spinal cord injury. *Cell Transplant* 24(4):661–672.
58. Snyder EY, Teng YD (2012) Stem cells and spinal cord repair. *N Engl J Med* 366(20): 1940–1942.
59. Committee on Care and Use of Laboratory Animals (1996) Guide for the Care and Use of Laboratory Animals (Natl Inst Health, Bethesda), DHHS Publ No (NIH) 85-23.
60. Lavik E, Teng YD, Snyder E, Langer R (2002) Seeding neural stem cells on scaffolds of PGA, PLA, and their copolymers. *Methods Mol Biol* 198:89–97.
61. Grayson AC, Cima MJ, Langer R (2005) Size and temperature effects on poly(lactic-co-glycolic acid) degradation and microreservoir device performance. *Biomaterials* 26(14):2137–2145.